Available online at www.sciencedirect.com

ScienceDirect

journal homepage: www.elsevier.com/locate/he

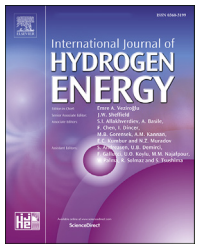

An evaluation of direct dimethyl ether (DME) synthesis from hydrogen and carbon dioxide based on CFD reactor simulations

Nils Beltermann [a,*], *Stefan Weiske* [a], *Rafael Becka* [a], *Remzi Can Samsun* [a], *Ralf Peters* [a], *Detlef Stolten* [b,c], *Thomas E. Müller* [d]

[a] *Electrochemical Process Engineering (IEK-14), Forschungszentrum Jülich GmbH, 52425 Jülich, Germany*
[b] *Techno-economic Systems Analysis (IEK-3), Forschungszentrum Jülich GmbH, 52425 Jülich, Germany*
[c] *Chair for Fuel Cells, RWTH Aachen University, 52072 Aachen, Germany*
[d] *Carbon Sources and Conversion, Ruhr-Universität Bochum, Universitätsstraße 150, 44801 Bochum, Germany*

HIGHLIGHTS

- Extensive model validation varying kinetic model as well as EoS.
- Parameter optimization over a wide range of parameters.
- Locally resolved gradients in membrane reactor.
- Developed optimization workflow.

ARTICLE INFO

Article history:
Received 8 December 2022
Received in revised form
12 April 2023
Accepted 25 May 2023
Available online 19 June 2023

ABSTRACT

To mitigate the effects of anthropogenic climate change, various options for decarbonizing the transport sector are under investigation. One promising approach is the chemical production of energy carriers and fuels from renewable sources. Among various options, dimethyl ether (DME) is discussed as one of the top candidates. However, the production of DME from a renewable raw material supply is associated with certain challenges. This study analyzes the direct synthesis of DME from CO_2 and H_2 based on computational fluid dynamics (CFD) simulations of the relevant reactors. For the CFD simulations, the software ANSYS Fluent was applied. Kinetic models were integrated by user-defined functions to describe the multiple heterogeneous catalyzed reactions in the synthesis reactor. Several kinetic models were tested with respect to their accuracy and applicability with regard to describing DME formation. A quasi-isothermal reactor model was implemented as base case. It is shown that the progressive formation of water slows down the reaction of direct DME formation. Moreover, a model for a membrane reactor was developed and analyzed in detail. In comparison to the base case, a significant increase in reactor performance was obtained. In conclusion, it can be stated that, for the direct conversion of CO_2 to DME, techniques for reducing the accumulation of water need to be adopted such as *in-situ* water removal or implementing an upstream reverse water-gas shift reactor.

* *Corresponding author.*
E-mail address: n.beltermann@fz-juelich.de (N. Beltermann).

https://doi.org/10.1016/j.ijhydene.2023.05.260

Introduction

According to the fifth special report on climate change from the Intergovernmental Panel on Climate Change (IPCC), the recent change in climate is extremely likely (95–99% probability) to have been caused by human activities [1, p.13-15]. The main cause for anthropogenic climate change is the emission of greenhouse gases (GHGs) – especially carbon dioxide (CO_2) – that emanate from the combustion of fossil energy carriers such as coal, oil and natural gas [2, p.18]. Therefore, the Paris Agreement [3] was ratified by the United Nations in 2015 with the goal of ensuring that the global temperature increase would not exceed 2 °C compared to the pre-industrial period.

The transport sector has seen stagnating development over the last 30 years, with a minor reduction in CO_2 emissions of only −0.8% (2018) against the base value of 1990 [4, sheet10].

Power-to-X connects to this consideration and entails the use of volatile renewable energy to synthesize renewable energy carriers, fuels and chemicals [5] *via* the electrolysis of water and carbon capture processes [6,7].

This paper focuses on the synthesis of dimethyl ether (DME), which is regarded as a promising candidate for diesel substitutes to be used in compression ignition engines [8, p.797]. DME exhibits the characteristics and properties of an appropriate diesel substitute. Its main characteristics include a high cetane number (>55) [9], no direct C–C bond and a high oxygen content (34.8 mass-%) [8]. Therefore, it produces considerably less pollutants like hydrocarbons, smoke and particulate matter than conventional fuels [10]. Furthermore, DME provides high energy density and can be liquefied under slightly elevated pressure [9,11]. The high vapor pressure in combination with a clean combustion makes DME a promising fuel substitute [9,10]. Moreover, DME can be blended with LPG or used with little adaptions to the injection system [9]. Azizi et al. [12] prepared a detailed literature study of the production processes for DME. The reactions involved in DME synthesis are listed in Table 1.

DME can be synthesized by two different processes. The conventional process for producing DME is the dehydration of methanol (eq. 4) [14], which is called the indirect process [12]. The more innovative method is the direct process [12] and utilizes syngas to form DME. Methanol is part of both pathways, and therefore directly couples the synthesis of DME to the synthesis of methanol.

In terms of CO_2 utilization and the production of fuels from renewable hydrogen, the production of DME based on syngas becomes an interesting option. While sustainable carbon sources are readily available [15], hydrogen supply chains and its distribution are discussed in detail by Hermesmann et al. [16] and Tsiklios et al. [17]. The motivation for direct conversion of CO_2 and H_2 to DME is clear on the basis of a short analysis of the related chemical equilibria. The conversion of CO_2/H_2 to methanol is limited by equilibrium limitations [5]. In case of concurrent methanol conversion to DME these limitations can be overcome and significantly higher conversions can be can be obtained [18].

A process design for direct DME synthesis from hydrogen and carbon dioxide is presented in Pontzen et al. [19] and Otto [20]. The CO_2-based production of DME was also part of the ALIGN CCUS research project [21]. Reviews of these specific topics of direct DME synthesis have been published by Frusteri et al. [22] and Alvarez et al. [23]. Poto et al. [24] and Park et al. [25] carried out process simulations with subsequent techno-economic evaluation of direct DME synthesis including the effect of membrane reactors. Hamedi et al. [26] published kinetic insight into several reactors involved in DME synthesis being integrated into a process model.

Various kinetic models for the synthesis of methanol and DME have been developed in recent years. For methanol synthesis, Bozzano et al. [27] published a detailed review of production technologies that includes an overview of kinetic models for methanol synthesis. In the case of DME synthesis, the model developed by Bercic and Levec [28] is the most prominent one featured in the literature [11,29–34].

In recent years, various authors have published studies regarding the modeling of DME synthesis reactors. The simplest way to describe DME synthesis from H_2 and CO_2 is to consider the chemical equilibrium. These thermodynamic evaluations exclude the reaction kinetics and provide no information about the design of the actual reactor. Ateka et al. [35] performed a thermodynamic study of direct DME synthesis with a focus on the co-feeding of CO_2. Their main finding is that the additional methanol consumption due to the dehydrogenation of methanol to DME increases the carbon dioxide conversion.

A common approach for the modeling of DME reactors is the development of one-dimensional (1D) reactor models. Vakilli et al. [36,37] performed optimizations for related 1D reactor models. De Falco et al. [38] carried out a thermodynamic analysis on 1D DME reactor model, concluding that the kinetic limitations of the DME synthesis can only be overcome through the removal of H_2O. Experimental and simulative studies of Otalvaro et al. [39] revealed a ratio of 3 between CZA (Methanol synthesis catalyst) and γ-Al_2O_3 (DME synthesis catalyst) to be optimal for direct DME synthesis from CO_2 rich syngas and stated *in-situ* water-removal as the main challenge. McBride et al. [40] present an analysis of DME synthesis with a spatially-patterned catalyst, stating that in the case of DME synthesis, a spatially-patterned catalyst does not reach the productivity of a well-mixed fixed bed because of increased methanol production. So far, a fully developed 3D

Table 1 – Reactions involved in direct DME synthesis [13].

Name	Chemical equation			ΔH^0_{298} [kJ/mol]	
CO hyd.	$CO + 2H_2$	⇌	CH_3OH	−90.6	1
CO_2 hyd.	$CO_2 + 3H_2$	⇌	$CH_3OH + H_2O$	−49.5	2
rWGS	$CO_2 + H_2$	⇌	$CO + H_2O$	41.2	3
MeOH deh.	$2\ CH_3OH$	⇌	$CH_3OCH_3 + H_2O$	−23.4	4

reactor model has only been published by Moradi et al. [41]. This reactor model featured an industrial scale reactor and followed a heterogeneous modeling approach.

Membrane reactor models have been published by various authors as an extension of the fixed bed reactors for DME synthesis. One of the first studies concerning membrane reactors for DME synthesis was by Iliuta et al. [42], who modeled a 1D plug-flow reactor in non-steady state conditions. Following a similar approach, Poto et al. [43] and De Falco et al. [44] simulated a 1D plug flow reactor with a tubular membrane for the *in-situ* removal of H_2O. Simulation results of both groups showed the beneficial effect of *in-situ* product separation in CO_2-based DME synthesis. These analyses are strikingly similar to the one presented here and, moreover, different reactor models and methodologies have been used. A simulative study of Koybasi and Avci [45] using a 2D microchannel membrane reactor showed a 2-fold increase of DME yield due to the use of a membrane for water removal. Guffanti et al. [46] and Iranshahi et al. [47] studied another possibility of *in-situ* water removal in DME synthesis reactors. The integration of water adsorbents aim at binding water from synthesis and therefore cause a similar effect as the integration of water-permeable membranes.

The motivation of the current publication and the identified research gap can be explained by the following:

In the literature, mainly basic 1D reactor models for the direct synthesis of DME from CO_2 are available. In this publication, 2D models are developed to show the impact of concentration gradients on water transport especially in the membrane reactor.

The presented methodology includes the model's development and validation in a more extensive manner than available publications. This step is mostly neglected in the literature. Most of the presented studies merely use the given models or present their own reaction models, which cannot be verified by the reader, thus negating the possibility of reproducing of the simulations.

Reactor modeling and methodology

The developed model merges various approaches into one single model. In the following, the different implemented models and boundary conditions are described.

Reactor models

From the variety of established and innovative reactors presented in the literature review, two different reactor types were chosen for further investigation. A quasi-isothermal system based on a Lurgi-type reactor (LR) for methanol synthesis was used for a base case simulation of the direct DME synthesis. The geometric data was taken from Samimi et al. [48], who modeled an industrial-scale methanol reactor in Shiraz (Iran). One tube of this reactor had a length of 7022 mm (+300 mm for inlet and outlet) and a diameter of 38 mm. These are industrial scales and, to achieve high levels of productivity, several thousands of these tubes were combined in one reactor (here: 2793). As all of the tubes have nearly the same operating conditions, a reduction of the given simulation problem to one single tube, which is symmetrical, is reasonable. The second reactor model is further derived from the Lurgi-type reactor. It integrates a semi-permeable membrane into the reactor and in this way becomes more sophisticated. This membrane reactor (MR) was chosen because water production seems to be the most crucial issue in direct DME synthesis from carbon dioxide and the membrane reactors seem to be the most suitable for overcoming this issue *via* the *in-situ* removal of water. The extended geometry is based on the quasi-isothermal reactor model so that in both cases, the same amount of catalyst material is present in the reaction zones. The geometries of both reactor models are displayed in Fig. 1.

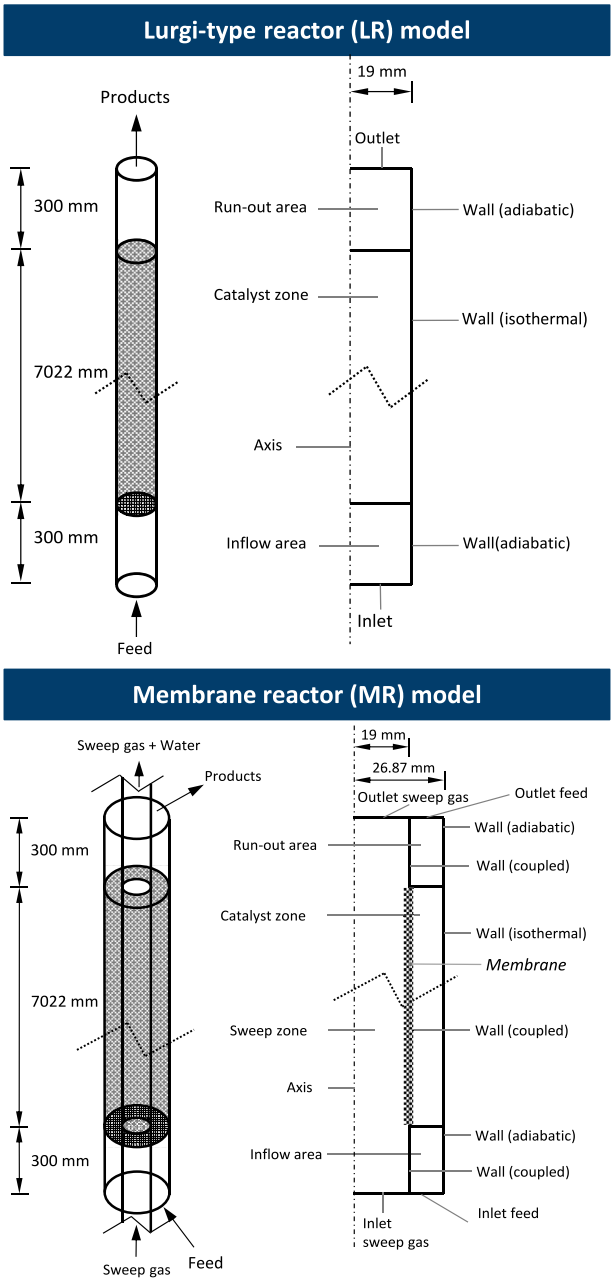

Fig. 1 – Geometry of Reactor models that were applied for analysis of the direct DME synthesis.

The reactors were cooled through the outer walls of the reaction zones. Based on this assumption, these walls were defined as being isothermal, which refers to the temperature of the cooling fluid. In this case, the temperature of the cooling fluid and that of the outer shell of the reactor wall are the same. This assumption leads to a simplification of the heat transfer by not modeling the heat conduction inside the tube wall in detail. Through this simplification, it is clear that an overestimation of the heat flux was made. As the analyzed reactors are quasi-isothermal, only small deviations in temperatures occur and the simplification is reasonable. Nevertheless, this model is limited with respect to the prediction of hot spots along the tube. The membrane is heat-coupled so that there can be a heat flux over the membrane. As the temperature of the feed gas and sweep gas are identical and the temperature control of the reactors is particularly good, there are only negligible heat fluxes. All other walls are adiabatic. The walls of the reactor models have no thickness (see Fig. 1) because the implemented heat transfer model of ANSYS Fluent uses a three-layer approach to determine the heat flux. The assumed theoretical thickness of the walls is set to 3 mm.

A mesh study of the presented reactor models was performed and is described in detail in Table S1 and Table S2. The element size was varied between 0.25, 0.5, 2 and 4 mm, which led to only minor relative deviations concerning the pressure loss (<0.6%) and carbon conversion (<0.1%). These results show that the implemented model is independent of the used mesh within the varied parameter range. With regard to calculation time, the mesh with element size of 0.5 mm was selected. In all meshes, inflation with growth rate of 1.2 close to boundaries is applied.

Kinetic modeling

Kinetic modeling allows a precise insight into the processes inside the reactor. In heterogeneous catalysis the kinetic rate equations are usually given in intrinsic form. That means the reaction rate is normalized on a certain mass of catalyst. The kinetic rate equations in heterogeneous catalysis are usually quite complex in order to cover the complex mechanisms happening at the catalyst. They usually consist of a kinetic term, a driving force and an adsorption term. Dealing with equilibrium restricted reactions, usually an equilibrium constant is integrated into the kinetic rate equation. The equilibrium constant for a reaction is not model-specific for one kinetic model. The equilibrium constants applied in this study are taken from Graaf [49] for methanol synthesis and Diep et al. [50] for methanol dehydration, respectively. Their mathematical expressions are listed in Table 2.

Table 2 – Equations for calculating the equilibrium constants that were applied in this study [49,50].

$\log_{10}(K_{eq,CO-hyd.}) = \frac{5139}{T} - 12.621$	5
$\log_{10}(K_{eq,rWGS}) = \frac{-2073}{T} + 2.029$	6
$K_{eq,CO_2-hyd.} = K_{CO-hyd.} \cdot K_{rWGS}$	7
$\ln(K_{eq,DME}) = \frac{2835.2}{T} - 1.675\ln(T) + 2.39\cdot10^{-4}T + 0.21\cdot10^{-6}T^2 + 13.36$	8

Beside the equilibrium constants kinetic rate equations comprise several adsorption terms, kinetic parameters etc. These terms and parameters are model-specific and only valid for the corresponding model. The models for the kinetic rate equations investigated in this study are listed in combination with a short description and the determining equation in Table 3. Because of the enormous number of model-specific parameters connected to the rate equations, they are not listed in this publication. They can be looked up in the supplementary materials in Table S3 to Table S6.

Modeling approach for mass transport limitations

As the approach for modeling the catalyst bed is pseudo-homogeneous, the direct interactions between the catalyst particles and bulk phase are not considered. The resistance parameters adopted in the model for the catalyst bed are provided in Table 4. They result from application of Ergun's law [61] to the industrial catalyst configuration provided by Samimi et al. [48] having a particle diameter of 5.47 mm with a bed voidage of 0.39.

According to the theory of heterogeneous catalysis, gradients in species concentrations can occur between the bulk fluid phase through a diffusive layer around the catalyst particles and the inside of the pore structure of the catalyst [63, p.10]. Decreased reactant concentrations lead to a decrease in the actual reaction rates and therefore must be considered in the modeling approach. Lommerts et al. [64] have analyzed many different ways of modeling these mass transport limitations in methanol synthesis and came to the conclusion that simple modeling by the Thiele modulus is appropriate for methanol synthesis. On basis of this simplified Thiele modulus, the internal efficiency factor is calculated by equation 18 [64] and equation 19 [65].

$$\eta_{int,i} = \frac{1}{\Phi_M}\frac{3\Phi_M\coth(3\Phi_M) - 1}{3\Phi_M} \quad 18$$

$$\Phi_M = \frac{r_P}{3}\sqrt{\frac{k_T(K_{eq,e}+1)}{D_{m,i}K_{f,e}}} \quad 19$$

For the external mass transport limitations through the diffusive layer, an external efficiency factor is defined by the second Damköhler number (Da_{II}) and equation (20) [66, p.146]. The second Damköhler number refers to the speed of reaction, in relation to the diffusive mass transport in the boundary layer (equation (21)) [67, p.224].

$$\eta_{ext,i} = \frac{1}{1+Da_{II}} \quad 20$$

$$Da_{II} = \frac{K_{T,eff}}{A_{ext}\beta_i} \quad 21$$

In the literature review, no reports were found that include mass transport limitations in the synthesis of DME in a pseudo-homogeneous modeling approach. As the indicated modeling approach was developed for methanol synthesis and methanol synthesis is a crucial factor for the direct synthesis of DME, the developed methanol model will be enhanced by a DME synthesis free of mass transport

Table 3 – Kinetic models with key information and equations describing the rate determining step in subsequent validation.

Product	Kinetic model	Highlights and reason for selection	Kinetic rate equation	
Methanol	Graaf [51]	• Simple model	$r_{CO-hyd.} = \frac{k_{kin,CO}K_{ads,CO}\left(f_{CO}f_{H_2}^{1.5} - \frac{f_{MeOH}}{f_{H_2}^{0.5}K_{eq,CO}}\right)}{(1+K_{ads,CO}f_{CO}+K_{ads,CO_2}f_{CO_2})\left(f_{H_2}^{0.5}+\frac{K_{ads,H_2O}}{K_{ads,H_2}^{0.5}}f_{H_2O}\right)}$	9
		• Widely applied in the literature [32–34,52–57]	$r_{CO_2-hyd.} = \frac{k_{kin,CO_2}K_{ads,CO_2}\left(f_{CO_2}f_{H_2}^{1.5} - \frac{f_{MeOH}f_{H_2O}}{f_{H_2}^{1.5}K_{eq,CO_2}}\right)}{(1+K_{ads,CO}f_{CO}+K_{ads,CO_2}f_{CO_2})\left(f_{H_2}^{0.5}+\frac{K_{ads,H_2O}}{K_{ads,H_2}^{0.5}}f_{H_2O}\right)}$	10
		• Two active sites (CO_2 and CO)	$r_{rWGS} = \frac{k_{kin,rWGS}K_{ads,CO_2}\left(f_{CO_2}f_{H_2} - \frac{f_{H_2O}f_{CO}}{K_{eq,rWGS}}\right)}{(1+K_{ads,CO}f_{CO}+K_{ads,CO_2}f_{CO_2})\left(f_{H_2}^{0.5}+\frac{K_{ads,H_2O}}{K_{ads,H_2}^{0.5}}f_{H_2O}\right)}$	11
	Bussche and Froment [58]	• Often used [53,54,59], also in combination with DME kinetic by Bercic and Levec [29]	$r_{CO_2-hyd.} = \frac{\kappa_4 p_{CO_2}p_{H_2}\left(1-\frac{1}{K_{eq,CO_2}}\frac{p_{H_2O}p_{MeOH}}{p_{H_2}^3 p_{CO_2}}\right)}{\left(1+\kappa_3\frac{p_{H_2O}}{p_{H_2}}+\kappa_1 p_{H_2O}^{0.5}+\kappa_2 p_{H_2O}\right)^3}$	12
		• Methanol formation only by hydrogenation of CO_2	$r_{rWGS} = \frac{\kappa_5 p_{CO_2}\left(1-K_{eq,rWGS}\frac{p_{H_2O}p_{CO}}{p_{CO_2}p_{H_2}}\right)}{\left(1+\kappa_3\frac{p_{H_2O}}{p_{H_2}}+\kappa_1 p_{H_2O}^{0.5}+\kappa_2 p_{H_2O}\right)}$	13
	Seidel et al. [60]	• Innovative transient kinetic model	$r_{CO-hyd.} = k_{CO}p_{CO}p_{H_2}^2\left(1-\frac{p_{MeOH}}{K_{eq,CO}p_{CO}p_{H_2}^2}\right)\theta_1\theta_3^4$	14
		• Three active surface sites (CO_2, CO, H_2)	$r_{CO_2-hyd.} = k_{CO_2}p_{CO_2}p_{H_2}^2\left(1-\frac{p_{MeOH}p_{H_2O}}{K_{eq,CO_2}p_{CO}p_{H_2}^2}\right)\theta_2^2\theta_3^4$	15
			$r_{rWGS} = k_{rWGS}p_{CO_2}\left(1-\frac{p_{CO}p_{H_2O}}{K_{eq,rWGS}p_{CO_2}p_{H_2}}\right)\theta_2\theta_3$	16
DME	Bercic and Levec [28]	• Most commonly used [11,29–34] • Modified parameter set for low temperatures [11,29–31]	$r_{DME} = \frac{k_{DME}K_{ads,MeOH}^2(c_{MeOH}^2 - c_{H_2O}c_{DME}/K_{eq,DME})}{(1+2(K_{ads,MeOH}c_{MeOH})^{0.5}+K_{ads,H_2O}c_{H_2O})^4}$	17

Table 4 – Parameterization of pseudo-homogeneous fixed bed modeling.

Parameter [62].	Unit	Value
C1: Inertial resistance	m^2	4.165E-8
C2: Viscous resistance	1/m	2874.24

limitations. The values used for the catalyst efficiency factors are provided in Fig. S1.

Modeling the kinetic reaction schemes by user-defined functions (UDFs)

The reaction schemes were implemented in ANSYS Fluent by the use of self-developed user-defined functions (UDFs). In this way, the UDFs were executed during all iterations and in all cells placed in the respective catalyst zone of the reactor model. In the case of methanol synthesis, the kinetic models by Graaf [51], Bussche and Froment [58] and Seidel et al. [60] were used. In the case of the kinetic models by Graaf [51] and Seidel et al. [60], the fugacities of the different species were needed to calculate the reaction rates. In order to calculate the fugacities, the Redlich-Kwong equation of state was used. This equation of state requires some additional values, e.g., critical parameters for the temperatures and pressures of the species. The model of Bercic and Levec [28] works with the concentrations and can be easily read by ANSYS Fluent (see Table 3). For taking mass transport limitations into account, the catalyst efficiency factors described above were implemented (see Section 2.3). The mass fraction of each catalyst (for methanol or DME synthesis; indicated by subscript j) is mathematically represented by $X_{cat,j}$ and their density by ρ_j. The actual reaction rates were calculated by multiplication of the relevant efficiency factor, intrinsic reaction rates, catalyst densities and catalyst shares (equation (22)).

$$\mathbf{R_i} = \boldsymbol{r_i \rho_{cat,j} \eta_{cat,i} X_{cat,j}} \quad 22$$

A deactivation factor of the catalyst was not inserted into this stationary simulation due the long operation time (4–6 years) of both relevant catalysts reported by Dieterich et al. [68].

A detailed scheme of all interactions of ANSYS Fluent with the UDF is provided in Fig. S2.

Table 5 – Selected boundary conditions for direct DME synthesis with the ranges applied in the parameter variations.

Parameter	Unit	Base Case	Min	Max
Volume flow	$L_{STP}/kg_{Cat}h$	1500	650	6500
Temperature	°C	250	200	300
Pressure	Bar	50	30	70
H_2	vol%	75	75	75
CO_2	vol%	25	0	25
CO/CO_x	vol%/vol%	0	0	75

Table 6 – Setups selected for validation in methanol synthesis.

Setup	Model	Equation of State (EoS)
S1	Seidel et al. [60]	Fugacities by Soave-Redlich-Kwong (SRK) [71]
S2	Bussche and Froment [58]	Partial pressures by mass fractions
S3	Graaf [51]	Fugacities by Soave-Redlich-Kwong (SRK) [71]
S4	Graaf [51]	Fugacities by Redlich-Kwong (RK) [72]

Boundary conditions

The selected boundary and operating conditions affect the outcome of the simulations, and so the selection of these parameters must be assessed. The volume flow of the feed gas is adapted from the work of McBride et al. [40], who give a range between 650 and 6500 $L_{STP}/kg_{cat}h$. A temperature of 250 °C and a pressure of 50 bar are common operating conditions for direct DME synthesis as can be seen in the review of Azizi et al. [12]. With respect to this, these conditions are defined as base case operating conditions in this study. The focus of this paper is the direct conversion of carbon dioxide and hydrogen into DME. From this perspective, a molar H_2:CO_2 ratio of 3 was chosen to start the investigations. A summary of the used operating conditions is given in Table 5.

In the following analyses, the compositions of the feed gas are changed through an increased amount of carbon monoxide. From a technical point of view, these different compositions can be supplied by the utilization of a reverse water-gas shift (rWGS) process with water removal.

Basic indicators

Different indicators are used for the evaluation of reactor performance in the various simulations. As examples of basis indicators for process engineering the conversion X_i, yield Y_{ij}, selectivity S_{ji} and space-time yield (STY) are defined by equation (23)–(26) [69, p.60]

$$X_i = \frac{n_{i,0} - n_i}{n_{i,0}} \tag{23}$$

$$Y_{ji} = -\frac{n_j - n_{j,0}}{n_{i,0}} \frac{\nu_i}{\nu_j} \tag{24}$$

$$S_{ji} = -\frac{n_j - n_{j,0}}{n_{i,0} - n_i} \frac{\nu_i}{\nu_j} = \frac{Y_{ji}}{X_i} \tag{25}$$

$$STY = \frac{n_j - n_{j,0}}{tV_R} \tag{26}$$

Results and discussion

The reactor simulations begin with validation studies concerning methanol and DME synthesis models (see Chapter 3.1). In addition to the selection of suitable kinetic models, a variation of equations of state was performed to see whether a simplified model with an easier application to DME synthesis (Redlich-Kwong, RK) could be used instead of Soave-Redlich Kwong (SRK). Such an extensive validation presented in this publication is a unique feature of this study. After the modeling approach was validated, simulation studies of direct DME synthesis were performed and an optimization workflow was conducted.

Validation of the simulation model

The selected kinetic models for methanol and DME synthesis shown in Table 3 were investigated with respect to their accuracy in this chapter. Manenti et al. [70] show that the combination of two approaches is common practice and an appropriate methodology. This methodology refers to a bifunctional catalyst, which provides active sites for methanol and DME synthesis and can be simplified as a physical mixture of both catalysts. As there must be two independent kinetic models integrated into the modeling approach, both of the models are first validated alone and merged subsequently.

Validation of the methanol synthesis model

The validation of the kinetic model for methanol synthesis is based on comparing the deviations between the prediction obtained in the simulations and experimental data from Samimi et al. [48], who published data on an industrial quasi-isothermal methanol reactor with a GHSV of 6248.2 h^{-1}. Referring to Dietrich et al. [68] this is a typical value for methanol synthesis applications and consequently applied in the validation study. Four different setups and kinetic models were tested in this validation study (see Table 6).

The deviations between the output data from this simulation study and the experimental data from Samimi et al. [48] are plotted in Fig. 2. The first simulation setup (S1) shows the largest deviations, which by far exceed the acceptable error limits (<5%). Setup S2 improves the overall accuracy, but in the case of carbon monoxide there is still an extremely high deviation of 17.9% relative to the experimental values. It can be seen from Fig. 2 that the modeling approach with the model by Graaf [51] and SRK (S3) seems to represent the simulations with the highest predictive accuracy. The maximum deviation is 3.4% for carbon monoxide. If the simpler EoS of RK is used (S4), this error slightly increases to 5.7%, but this setup is much easier to apply to a more complex mixture with DME (no intermolecular forces required as input in case of RK). From this perspective, the Setup S4 was chosen to be the base model for the direct DME synthesis due to a good accuracy combined with good applicability in ANSYS Fluent. Furthermore, the

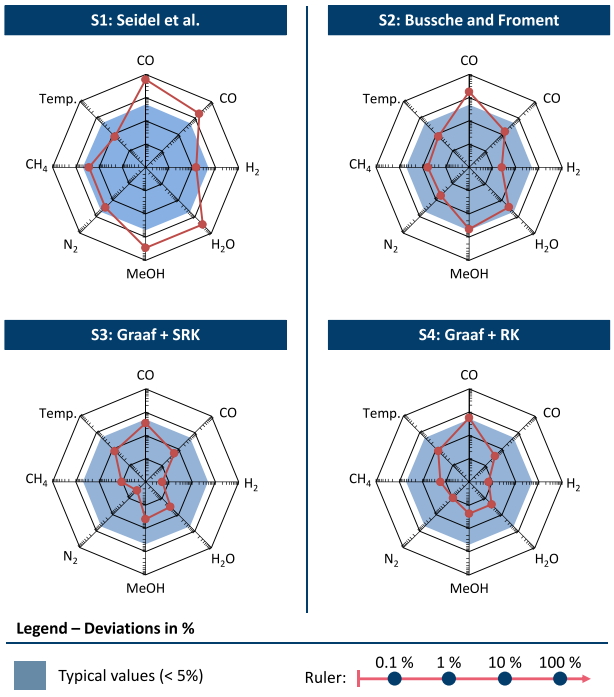

Fig. 2 – Deviations between the CFD simulations in this study and experimental data from Samimi et al. [48] under reference conditions listed Table S7.

Table 7 – Parameterization of DME synthesis kinetic by Bercic and Levec [28] (Full information in Table S6).

Parameter	Unit	Original [28]		Modified [11,29–31]	
		A_i	B_i	A_i	B_i
k_{DME}	kmol/kg*h	$5.35x10^{13}$	−17280	$3.7x10^{10}$	−105000
$K_{ads,CH3OH}$	m^3/kmol	$5.39x10^{-4}$	8487	$7.9x10^{-4}$	70,500
$K_{ads,H2O}$	m^3/kmol	$8.47x10^{-2}$	5070	$8.4x10^{-2}$	41,100

model of Graaf [51] is widely used in modeling studies which makes this selection a reliable setup for following studies.

Validation of the DME synthesis model

A frequently used model [11,29–31] to describe methanol dehydration was developed by Bercic and Levec [28]. In addition to the original model, there have been modifications to adapt the original model to operating conditions with lowered temperatures [11,29–31]. All of parameterizations can be seen in Table 7. The results of the validation can be seen in Fig. 3.

The modified parameterization is more accurate than the original across the entire temperature range. Comparing the simulations to the experimental results of Ghavipour et al. [74] at the high GHSV (19,905 h^{-1}) a close understanding of kinetic phenomena in of DME synthesis can be generated. At increased temperatures, the experiments come closer to chemical equilibrium (around 80% conversion), where the modified setup in particular shows exceptionally good agreement with a deviation of ca. 2% at 350 °C. The average deviation of the modified setup was 24% and therefore much better than the original setup (ca. 58%). Because of this behavior and the recent common usage in the literature leading to the same

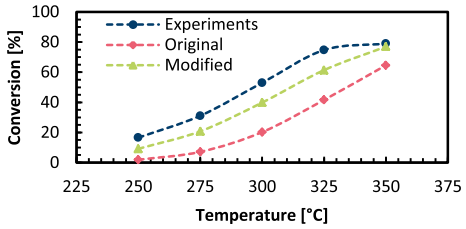

Fig. 3 – Selection of parameterization for the kinetic model of methanol dehydration by Bercic and Levec [73], with experimental data from Ghavipour et al. [74]. Feed stream of methanol: 30 $g_{MeOH}/g_{cat}h$ at 3 bar.

conclusion, the modified parameterization is chosen for use in simulation studies. Therefore, by selecting the widely used kinetic models for methanol synthesis as well as DME synthesis by analyzing their accuracy compared to experiments, a reliable model basis for further studies is provided.

Simulation studies

After building up the model in the previous sections, the simulation studies will be performed in the following sections. Doing this, an optimization workflow is followed investigating different operation conditions and catalyst setups. As the last - and most complex optimization-a membrane is inserted. The following sections are named after the parameter/setting optimized.

Direct DME synthesis from hydrogen and carbon dioxide

For the direct synthesis, the described models for methanol and DME synthesis are merged. The temperature of the base case is set to a typical 250 °C being a typical value [12]. The volume flows (1000–3000 $L_{STP}/kg_{cat}h$) are adapted from McBride et al. [40], where these are set between 650 (equilibrium case) and 6500 $L_{STP}/kg_{cat}h$ (kinetic case). Fig. 4 shows the calculated conversions, STYs and selectivities of the base case simulation study.

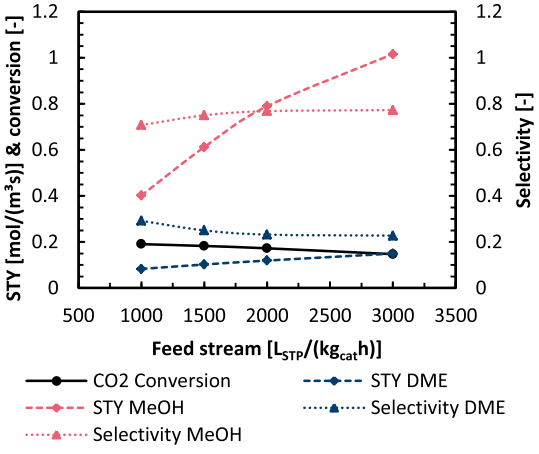

Fig. 4 – STYs, selectivities and conversions for base case simulations of direct DME synthesis from H_2 and CO_2 ($H_2/CO_2 = 3$, T = 250 °C, p = 50 bar).

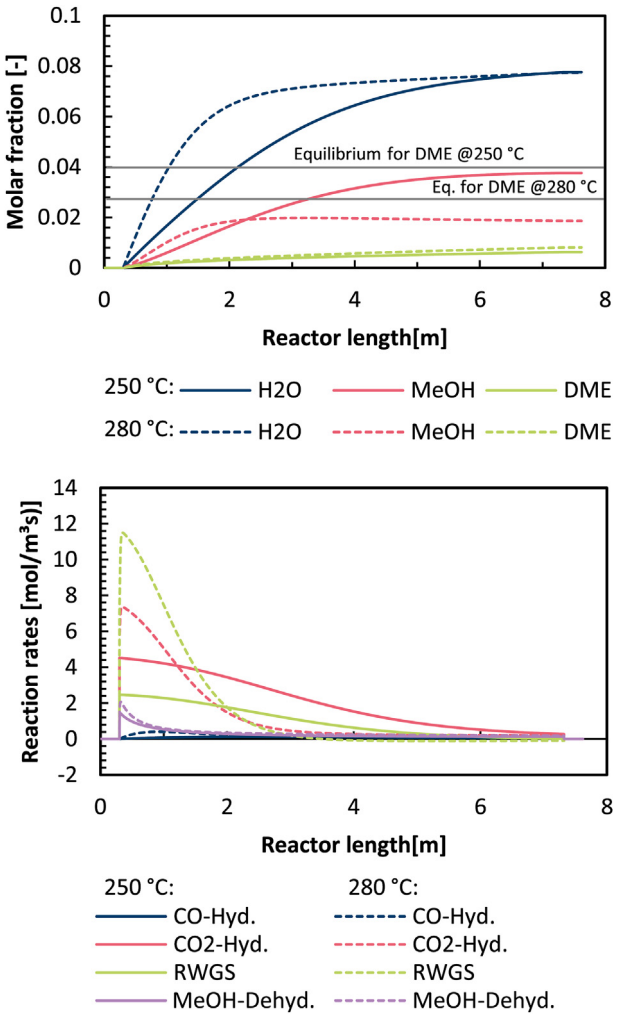

Fig. 5 – Reactor profiles, molar fractions of compound i (top) and reaction rates (bottom), derived for the base case simulation of direct DME synthesis from H_2 and CO_2 ($H_2/CO_2 = 3$, T = 250/280 °C, 50 bar, 1500 $L_{STP}/kg_{cat}h$).

The selectivity and space-time yields concerning DME are for all cases relatively low in comparison to the synthesis of methanol.

For further investigations of direct DME synthesis in this publication a feed flowrate of 1500 $L_{STP}/kg_{cat}h$ is selected which results in a GHSV of 1601 h^{-1}.

Even at low feed flow rates the amount of synthesized DME is low and far from the relevant equilibrium composition as can be seen in Fig. 5. Additionally, the reason for this particular behavior can be identified by the reactor profiles of molar fractions and reaction rates at different operating temperatures (see Fig. 5).

As shown in Fig. 5 water formation is very fast at the reactor inlet. Once the molar fraction of water reaches a certain value, the reaction rates drop significantly to the middle of the reactor (ca. 2 m). Thus, the formation of water seems to be the main reason for the low rates obtained in this base case scenario. Changes in operating temperature affected the profiles; increased temperatures led to faster kinetics. However, this did not significantly affect the DME productivity of the reactor which was inferred to be a consequence of the product inhibition resulting from the formation of water. In contrast to this, the productivity to methanol formation was strongly affected by a change in the operating temperatures. The simulation revealed substantial restrictions in direct DME synthesis. We would like to emphasize that it is a matter of kinetics and not thermodynamic limitations (Fig. 5, top).

In the following, the direct DME synthesis is analyzed in detail to develop concepts for improving reactor performance. For this purpose, a detailed simulation was conducted that includes variations in boundary and operating conditions, such as feed-gas compositions, temperatures, pressures and catalyst compositions.

Variation of feed gas composition. The formation of water is a result of the use of the CO_2-rich feedstock. If a certain fraction of the carbon source is replaced by CO, less water will be formed in the reactor. From this perspective, it seems reasonable to increase the CO content of the feed gas prior to the synthesis reactor. This can be done by upstream implementation of a water-gas shift reactor and concomitant water removal. The impact of an increased CO content in the feed gas is graphically depicted in Fig. 6.

The highest STYs of DME were achieved, when only CO was considered as the carbon source. In this case, the STY was 10.1 times higher than in the case of CO_2 as the sole carbon source. With increasing CO molar fraction in the feed gas stream, increased selectivity towards DME was obtained. Thus, the selectivity changed from 46.7% to 91.4% over the range covered in the simulation study. The introduction of CO to the feed stream had an overall positive impact on the direct DME synthesis. This relation was taken into account during the subsequent analyses by integrating three different feed gas compositions ($CO/CO_x = 0.25, 0.5, 0.75$). Moreover, the results show that by adjusting the operating temperature from

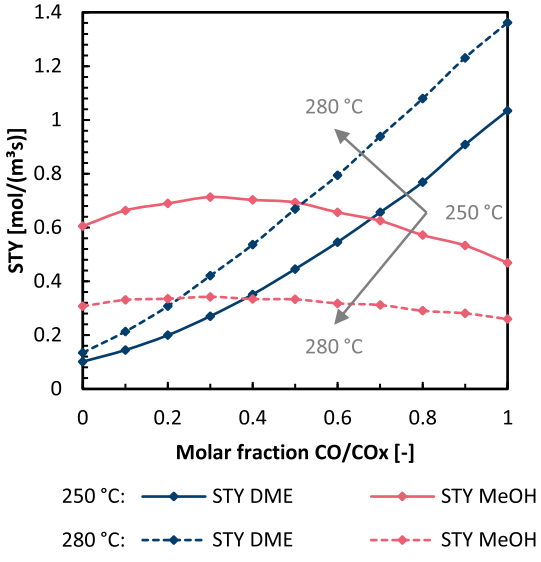

Fig. 6 – STYs of direct DME synthesis with increased CO/CO_2 ratios and two temperature levels (T = 250/280 °C, 50 bar, 1500 $L_{STP}/kg_{cat}h$).

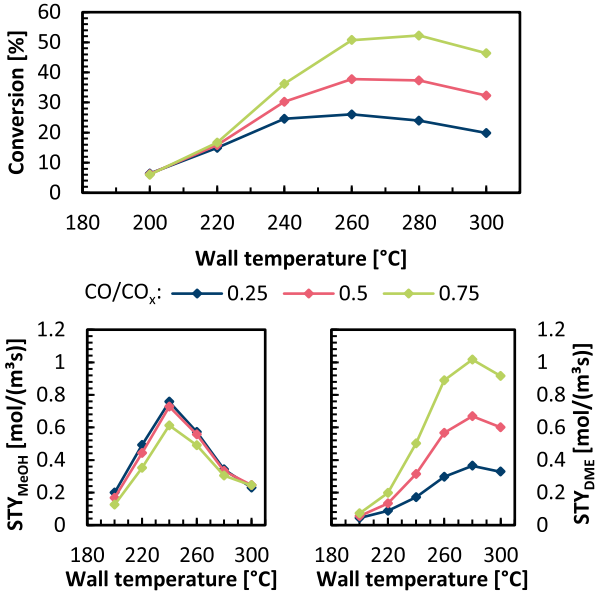

Fig. 7 – Conversion (top) and STYs for methanol and DME (bottom) in direct DME synthesis upon varying the wall temperature (T = 200–300 °C, 50 bar, 1500 $L_{STP}/kg_{cat}h$).

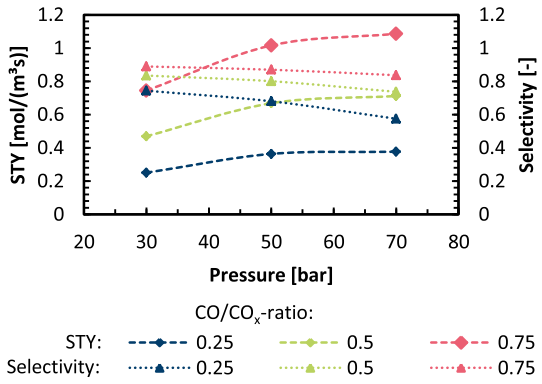

Fig. 8 – STY and DME selectivity for different operating pressures (p = 30–70 bar, 280 °C, 1500 $L_{STP}/kg_{cat}h$).

250 °C to 280 °C, the STY and selectivity of the DME synthesis increased (+44% on average). This simulation, thus, revealed that the operating temperature has a strong impact on the reaction kinetics of direct DME synthesis and must therefore be investigated in detail.

Simulation study concerning wall temperature. The goal of the next step of the simulation study was to determine the optimal operating temperature of a quasi-isothermal DME synthesis reactor. The optimal operating temperature is a trade-off between factors such as conversion and STY. This study is connected to the variations in feed gas composition described above and considers the same boundary conditions. The results of varying the operating temperature between 200 °C and 300 °C are shown in Fig. 7.

As can be seen from Fig. 7, a pronounced maximum in the STY of DME is observed at ca. 280 °C. The maximal conversion is dependent on the CO/CO_x-ratio and increases with a rise in temperature from 240 °C (CO/CO_x = 0.25) to 280 °C (CO/CO_x = 0.75). The consumption of methanol mitigates the optimal process temperatures towards lower ones. At the same time, the reaction rates of methanol dehydration decrease, when the reactor is operated at lower temperatures. Here, a central challenge in direct DME synthesis is once again visible. DME and methanol syntheses show different optimal operating conditions (240 °C and 280 °C) with steep decreases from the optimum. This leads to the conclusion that these two reactions do not match well in terms of temperature.

Simulation study concerning operating pressures. Aside from the operating temperature, the operating pressure can be adapted to maximize the performance of the synthesis reactor. For methanol synthesis, higher pressures are preferred because the increased pressure levels shift the chemical equilibrium towards the product side, i.e., methanol. As the methanol and DME synthesis are coupled in case of the direct DME synthesis, this trend is also valid for the latter. As a conclusion of the parameter study performed above, a temperature of 280 °C was chosen to be applied to the quasi-isothermal reactor. The results of the pressure variation are depicted in Fig. 8.

The space-time yield (DME) can be increased slightly (average + 5.6%) with increased pressures (here: 70 bar). The lowered pressures, on the other hand, lead to a more significant reduction in STY (- 29.1%). As the methanol synthesis is strongly affected by the pressure increase, the selectivity towards DME is simultaneously reduced at higher pressures (+5.3% higher at 30 bar and −9.1% lower at 70 bar compared with the base case at 50 bar). The previously selected operating pressure of 50 bar indicates the best compromise between the two divergent indicators and was therefore chosen to be applied in all further simulations.

Simulation study concerning catalyst properties. The last parameter study of the quasi-isothermal reactor model was designed to vary overall and spatially resolved catalyst distributions in the fixed bed. Firstly, the composition of the bifunctional catalyst was changed. The mass content of the DME catalyst was varied from 0.1 to 0.9, which means that the methanol catalyst content is anti-proportional. In the literature, values for the density of the bifunctional catalyst of 1783.5 kg/m^3 can be found, but no information is given about the mixture or method [31,70].

As a further simplification, both catalysts are assumed to have the density of 1750 kg/m^3. Based on this assumption, the volume and mass fractions of the two catalysts can be considered equal. The compositions in this first study are homogeneously distributed over the length inside the fixed bed. The results are visualized in Fig. 9.

The STY shows a wide plateau of between 0.3 and 0.7, where the changes in the catalyst compositions only slightly influence the STY. Apart from this plateau, the STY significantly decreases in low concentrations of DME or methanol catalysts. In contrast, for high selectivities towards DME, a reasonable amount of DME catalyst is required in the fixed bed. At ratios higher than 50% DME catalyst, there are only

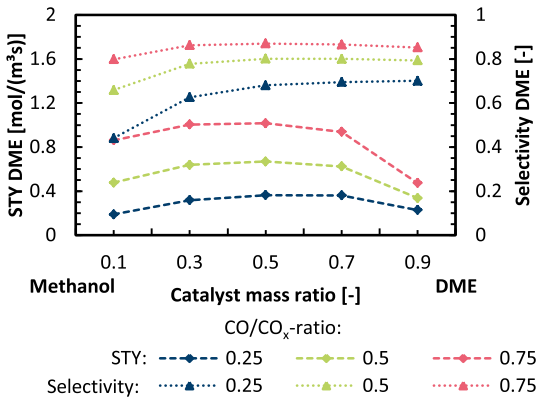

Fig. 9 – STY and selectivity to DME upon varying the mass ratio of methanol and DME catalyst (280 °C, 50 bar, 1500 $L_{STP}/kg_{cat}h$).

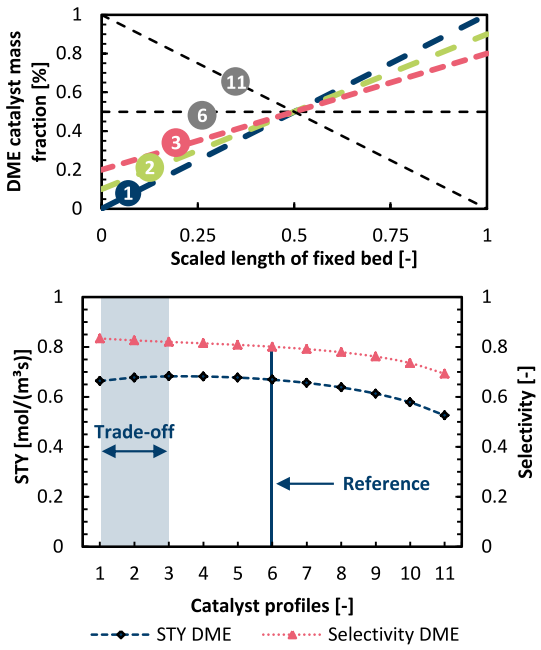

Fig. 10 – Top: Visualization of locally resolved catalyst profiles. Bottom: STY and DME selectivity for different locally resolved catalyst profiles (280 °C, 50 bar, 1500 $L_{STP}/kg_{cat}h$).

small potentials to increase the selectivity further (+2.6%). It seems that equally distributed (50:50) catalyst ratios are the best trade-off for this analysis. As an extension to the simulation study discussed, the distributions of the catalyst masses can be locally resolved; this means that the mass ratios can be adapted along the reactor length to adapt to the reaction conditions. In the course of this analysis, 11 different profiles for the catalyst distributions were implemented in the simulation model. Globally, all setups have an equal distribution of 50% DME and 50% methanol catalyst. The distributions are considered to change linearly and cut through the 50:50 distribution at the center of the fixed bed. To give an impression of the methodology used, only a few distributions are demonstrated in Fig. 10.

From a technical point of view, the locally resolved manufacturing of catalysts may seem challenging. Each layer must be adapted to the predefined catalyst mixture.

Nevertheless, this study is a theoretical simulation one in which the effects of such an approach can be easily calculated. The results of these variations are shown in Fig. 10.

The results reveal that it is best to start with a low DME catalyst mass fraction and further increase it along the fixed bed, as represented by profiles 1–3. This behavior can be explained by the fact that, for the dehydration of methanol to DME, methanol is needed in the first place and therefore a large amount of methanol catalyst at the beginning of the reactor is preferred. The results show that there are only small potentials to increase the STY *via* the locally-resolved catalyst mass fractions. The maximum STY is achieved by implementing profile number 3 and is calculated to be 0.682 mol/(m^{3}s). In comparison to the homogeneously-distributed catalysts (profile number 6), profile 3 has achieved a 2% increase in STY. In Fig. 10, the blue marked region shows high STY and selectivities, but the trends are opposing, which means that a trade-off between STY and selectivity must be made. The maximum selectivity is achieved by implementing profile number 1. Here, an increase of about 4.1% can be generated in comparison to profile number 6.

The shown results for direct DME synthesis are in agreement with the experimental study carried out by Otalvaro et al. [39]. For CO2-rich syngas ($CO_2/CO_x = 0.8$) they observe a methanol yield being 2 to 77 times higher than the DME yield. For CO-rich syngas ($CO_2/CO_x = 0.2$) their results show higher (around twice) DME yields compared to methanol yields while an elevated temperature of 260 °C was always beneficial for DME yield compared to 230 °C. Kurzina et al. [75] also found out a locally-resolved catalyst distribution with more methanol synthesis catalyst in the front and more DME catalyst in the latter reactor section to be beneficial referring to their experimental studies. They also detected no loss in DME yield for their experiments over 180 h.

Up to now, all of the outlined techniques have included the operating conditions and catalyst structure of the quasi-isothermal synthesis reactor. Furthermore, all of the calculated potentials are bound to a specific range because the main challenge of direct DME synthesis – the formation of water – remained untouched. In the following analysis, a membrane reactor setup is used to extract the product water from the reaction zone.

Analysis of in-situ *water removal by a semi-permeable membrane*

Based on the identified challenge of water formation in direct DME synthesis, a promising innovative reactor concept can be built on the principle of *in-situ* water removal using a semi-permeable membrane. The membrane reactor model is an extension of the developed quasi-isothermal reactor model. The results from all other simulation studies up to this point are used to define the boundary conditions. The chosen parameters are 280 °C, 50 bar and a volume flow of 1500 $L_{STP}/kg_{cat}h$. As the optimization of catalyst distributions has only minor

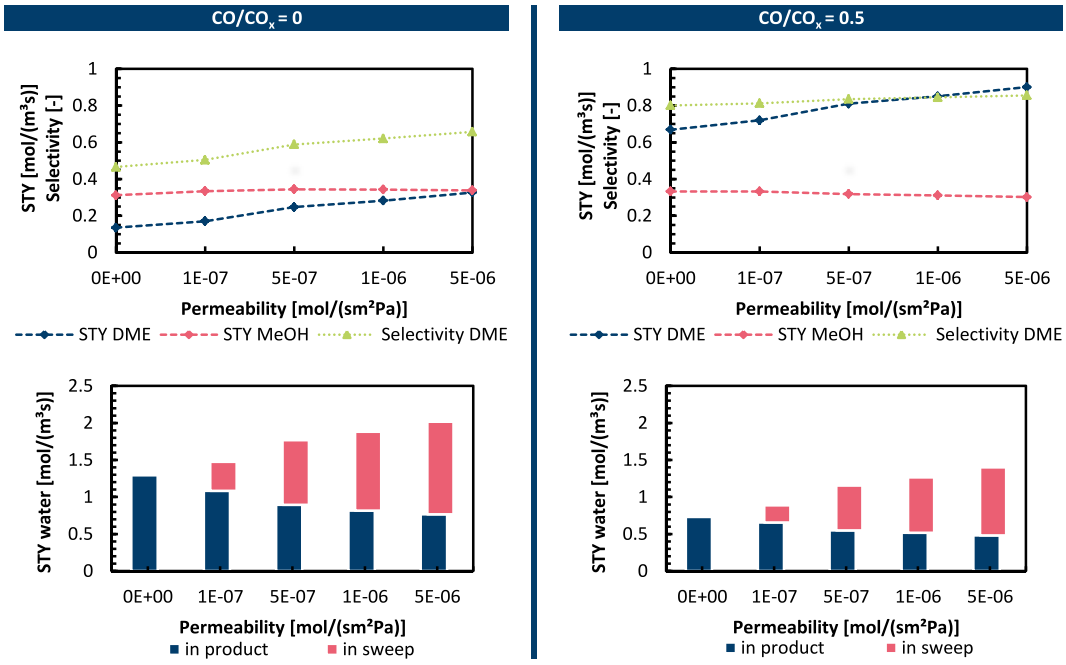

Fig. 11 – Impact of membrane permeability on the performance of the membrane reactor (280 °C, 50 bar, 1500 $L_{STP}/kg_{cat}h$, $S_w = 2$).

impacts on the reactor's performance, a homogenous distribution of the fixed bed is selected (50:50, profile 6). As a major additional boundary condition, the permeability of the membrane is introduced by the membrane reactor model. Rohde et al. [76] performed a literature survey, as well as experimental investigations, and identified the following reasonable operating performances for ZSM5 zeolite membranes.

- Permeabilities between 1E-07 and 1E-06 mol/(sm^{2}Pa)
- Selectivity $S_{H2O/H2}$ >10

The influence of this new parameter needs must be checked in a further simulation that includes a variation from 1E-07 to 5E-06 mol/(sm^{2}Pa). The maximum permeabilities are increased compared to the values in Rohde et al. [76]. This study aims to show the potential of the technology based on the state-of-the-art membrane and the potentials that could be unlocked by a further increase in membrane performance properties. The second newly-integrated boundary condition for modeling the mass flow through the membrane is the selectivity of the membrane. The selectivity of the membrane defines the ratio between the molar flow of water per molar flow of hydrogen.

The selectivity describes specifically the proportion of water that passes through the membrane. The basic value for the selectivity $S_{H2O/H2}$ is defined as 40 [44,76]. Promising results for *in-situ* water removal are also the outcome of investigations conducted by Gorbe et al. [77] who carried out experiments using zeolite membranes under methanol synthesis conditions obtaining separation factors of 55–250 for CO_2/H_2O and 12 to 150 for H_2/H_2O. Since this study is a reactor modeling study these membrane values are adopted and integrated into the model to show potential benefits provided by membranes. A detailed insight into the membranes is not in the scope of this publication. The maximum hydrogen loss of all simulations is calculated to be 0.000023% of the inserted hydrogen. This exceedingly small amount can be neglected in further studies. Moreover, the properties of the membrane, the boundary conditions of the sweep gas side are other crucial elements for the optimization of the membrane reactor. In the first simulation study presented in Fig. 11, the sweep gas flow was set to have a double molar flow ($S_w = 2$, see 27, below), as the reactor side needed to have enough capacity to transport the water out of the reactor.

$$S_W = \frac{\dot{n}_{sweep}}{\dot{n}_{Feed}} \quad 27$$

In the upper section of Fig. 11 the impact of permeability on the reactor performance is presented for two CO/CO$_x$-ratios. The bottom part of Fig. 11 provides a closer insight by showing the removed amount of formed water from the reaction zone by the membrane. Table 8 presents a summary of the optimized reactor concepts also including a variation of the sweep gas ratio.

In Fig. 11 it becomes obvious that the permeability of the membrane has a significant impact on the performance parameters as STY and selectivity. This is valid for pure CO_2 as well as CO/CO$_x$ ratio set to 0.5. The STY for DME is increased by 108.7% (pure CO_2) and 27.1% (CO/CO$_x$ = 0.5) respectively. The lower section of Fig. 11 explicitly states the ability to remove the formed water from the reaction section efficiently. In both cases, for a permeability of 1E-6 mol/(sm^{2}Pa) more than 50% of the formed water is leaving the membrane reactor in the sweep stream and is consequently removed from the reaction zone.

Beside the deeply investigated cases of Fig. 11 with a sweep gas ratio of 2, Table 8 contains results of an increased sweep

Table 8 – Results of multiple optimization strategies applied to the membrane reactor (280 °C, 50 bar, 1500 $L_{STP}/kg_{cat}h$, P_M = 1E-06 mol/(sm²Pa), $S_{H2O/H2}$ = 40, Profile 6). Space-time yield (STY) in mol/(m³s). Deviations (+Δ) in %.

Optimization		Volume flow ratio of sweep-gas to feed gas (S_w)						Catalyst	
Cases	Base	2		5		10		Profile 3 (S_W = 10)	
CO/CO_x	STY	STY	+Δ	STY	+Δ	STY	+Δ	STY	+Δ
0	0.136	0.283	108.7	0.337	148.5	0.366	169.9	0.381	181.0
0.5	0.669	0.850	27.1	0.887	32.6	0.912	36.4	0.919	37.4
0.75	1.016	–	–	–	–	–	–	1.160	14.2

gas ratio up to 5 and 10. This optimization also results in significant enhancement of STY of DME. Compared to the base case, for S_W = 10 enhancements of 169.9% (pure CO_2) and 36.4% (CO/CO_x = 0.5) can be achieved.

Due to the small potentials of the optimizations regarding the catalyst arrangements (Section 3.2.1.4) it has not been taken into account in the membrane investigation of this section so far. To finalize the optimization workflow the promising spatial catalyst setup following profile 3 (See Fig. 10) is applied to the feed streams studied. Even if the enhancements due to profile 3 are not that extensive, an increased STY for DME can be observed in every case. Additionally, one best case is defined where all optimization outcomes are combined. That means the locally resolved catalyst profile 3 in combination with the CO/CO_x-ratio of 0.75. The STY for DME in that best case is 1.16 mol/m³s. Especially in that case with high amounts (and consequently lowered water formation) the relative enhancement of STY is lower compared to the cases with lower CO amount in feed.

These results are in agreement with previously conducted studies. Although precise and absolute comparison is difficult due to the wide range of parameters and setting options,

De Falco et al. [44] obtained a similar enhancement of 31.5% of DME yield as effect of membrane insertion with a mixture of CO and CO_2 in the feed. The very high relative impact in case of pure CO_2 (here: 181.0% enhancement) compared to CO-rich feedstocks (here: 14.2% enhancement) is confirmed by the results of Iluta et al. [42] who stated an increase of above 200% for CO_2-rich case and significantly lower relative enhancement in case of high CO contents.

To gain a more detailed view of the mechanisms of water transport and to see possible further optimization potentials, multiple cross-sections along the reactor axis must be analyzed. A CO/CO_x-ratio of 0 leads to the highest water production in the reactor, as can be seen from Fig. 11.

These cases are used to analyze the water transport in a more detailed manner. Therefore, two positions are selected that provide information about the species concentrations orthogonal to the reactor axis. The cross sections are placed in the middle (x_1 = 3.811 m) and at the end of the fixed bed zone (x_2 = 7.322 m). The membrane reactor is symmetrical, so that in Fig. 12, only one half must be displayed in the radial direction. It is obvious that the diameter of the sweep zone is large in comparison to that of the reaction zone. The reason for this is the basic design of the quasi-isothermal reactor, which was used to design the model of the membrane reactor and is adapted from Samimi et al. [48] (see Chapter 2.1).

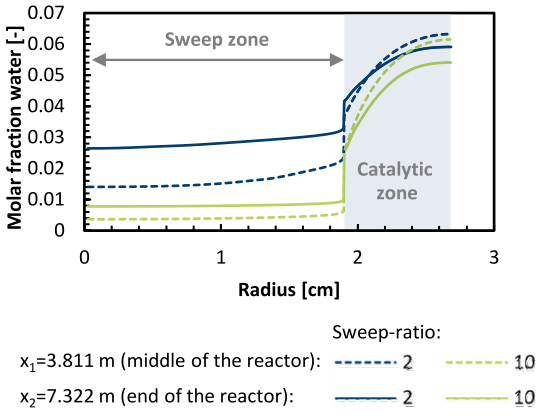

Fig. 12 – Molar fraction of water in radial direction of reaction mixture in the positions x_1 and x_2 inside the MR (280 °C, 50 bar, 1500 $L_{STP}/kg_{cat}h$, P_M = 1E-06 mol/(sm²Pa), $S_{H2O/H2}$ = 40).

An increase in the molar fraction of water in the sweep gas was expected and is proven by Fig. 12. The sweep gas flow rate has a notably strong effect on the radial profile in the catalytic zone. The driving force of this mass transport is reduced along the reactor length due to the decreasing difference in the partial pressure of water. In the case of the higher sweep gas stream, there were only small differences between the middle and end of the reactor on the two sides of the membrane, so that a further increase would only lead to a minor increase in water transport and reactor performance. Fig. 12 shows large gradients inside the catalytic zone. These gradients imply that the mass transport is already limited and the distance from the outer side of the reactor (wall) to the membrane is relatively large in terms of diffusive mass transport. If these mass transport limitations could be reduced, further potentials in the reactor could be achieved. As the formation of water is the main reason for the slowed down synthesis reaction, the reaction rates inside the catalytic zone of the membrane reactor have locally large gradients as well. Closer to the membrane, the reaction rates are up to eight times higher than those close to the wall. The first quarter of the catalytic zone close to the membrane produces nearly 55.3% of the total DME of the reactor. Based on this accumulated output, the asymmetrical usage of the catalyst can be described as inefficient. Further optimizations of the design can solve this issue, but are not a part of this paper.

Conclusions

In this study, the direct synthesis of DME from CO_2 and H_2 was evaluated based on CFD reactor simulations. The aim was to build up a model in ANSYS Fluent covering several modeling aspects and obtain good agreement with experimental data with regard to accuracy and applicability. With these advanced reactor models the operating conditions of the direct DME synthesis were optimized in relation to common performance indicators. The main conclusions from modeling and result perspectives are highlighted in the following bullet points:

- The model of Graaf shows the best accuracy in describing methanol synthesis compared to other models. The use of RK EoS instead of SRK EoS leads to an only minor loss in accuracy but simplifies the modeling and makes the Graaf model applicable to any feed composition. For DME synthesis the modified parameter set shows better accuracy compared to the original set.
- The kinetic study revealed that the reaction is heavily influenced by the formation of water. It is clearly pointed out that this issue is as much related to kinetics as to thermodynamics. The coupled production of water retards the formation of DME by methanol dehydration. Only low conversions can be obtained with a simple quasi-isothermal fixed bed reactor. Consequently, running the reaction to the equilibrium conversion is not suitable, as kinetic limitations lead to compositions of the reaction mixtures that are far from the chemical equilibria.
- Variations in the base case scenario revealed that there are large optimization potentials in changing operating conditions and catalyst distributions. Essentially, the increase in productivity stems mostly from introducing CO into the feed gas. With regard to CO_2 as the initial carbon source, this change in feed gas composition is readily supplied with an upstream rWGS reactor with concomitant water separation. Please note that this process combination requires heat at high temperatures (>700 °C) to be available for operating the rWGS reactor.
- As the presence of water is the main reason for the low productivity of direct DME synthesis reactors, *in-situ* removal of water through a membrane was explored as a counter measure. It was shown that the productivity of the reaction can be increased significantly, and, therefore, it is recommended to implement such water removal, if the direct pathway is to be realized. The membrane properties have a significant impact on reactor performance and, if the performance factors of the membranes increase, the membrane reactors offer additional benefits. A crucial aspect for the design of DME membrane reactors are the radial gradients in species concentrations that significantly influence the reaction rates. Based on these gradients, the reaction rates spatially differ. For achieving more homogeneous conditions, the ratio between the membrane surface and the catalyst volume must be increased.

All in all, several measures have been identified for enhancing the reactor performance in direct DME synthesis. Further studies will be directed to dealing with the kinetic inhibition of DME forming caused by water. Moreover, the promising approach of realizing a DME membrane reactor will be followed. Especially in this regard, CFD modeling is a relevant tool offering the possibility to change geometries without elaborate and time-consuming manufacturing of different reactor geometries.

Declaration of competing interest

There are no conflicts to declare.

Acknowledgements

The authors are grateful to their colleagues in the fuel synthesis departments at Jülich, as well as to all project and cooperation partners for the stimulating scientific exchange.

T.E.M. gratefully acknowledges funding of the endowed chair Carbon Sources and Conversion (CSC) by the state of North Rhine-Westphalia, grant number IRR-2018-1, RWE Power AG, and the Faculty of Mechanical Engineering of Ruhr-Universität Bochum.

Appendix A. Supplementary data

Supplementary data to this article can be found online at https://doi.org/10.1016/j.ijhydene.2023.05.260.

Nomenclature

List of abbreviations

1D	One dimensional
2D	Two dimensional
3D	Three dimensional
CFD	Computational fluid dynamics
DME	Dimethyl ether
EoS	Equation of State
EU	European Union
GHG	greenhouse gases
IPCC	Intergovernmental Panel on Climate Change
LPG	Liquefied petroleum gas
LR	Lurgi-reactor type
MR	Membrane-reactor type
RK	Redlich-Kwong
rWGS	Reverse water-gas shift
SRK	Soave-Redlich-Kwong
UDF	User-defined function

Latin symbols

A_i	Pre-exponential factor (Arrhenius equation) []
B_i	Factor Arrhenius rate []
c_i	Concentration of species i [mol/m^3]
D_{eff}	Effective diffusion coefficient [m^2/s]
d_p	Particle diameter [m]
f_i	Fugacity [bar]

GHSV	Gas hourly space velocity [h^{-1}]
k	Reaction rate constant []
$K_{ads,i}$	Adsorption constant [1/bar]
K_{eq}	Equilibrium constant [$Pa^{\sum v}$]
$\dot{n}_i$	Molar flow rate [mol/s]
p_i	Molar flow rate [mol/s] p_i Partial pressure [bar]
P_M	Permeability of the membrane [mol/(m^2sPa)]
R	Universal gas constant [1/(Kmol)]
r_i	Intrinsic reaction rate [mol/kgs]
R_i	Volumetric reaction rate [mol/(m^3s)]
S	Selectivity [–]
$S_{H2O/H2}$	Selectivity of the membrane [–]
STY	Space time yield [mol/(m^3s)]
S_w	Flow rate ratio of sweep to feed gas stream [–]
T	Temperature [K]
X	Conversion [–]
X_{Cat}	Catalysts mass fraction [–]
Y	Yield [–]
y_i	Molar fraction [–]

Greek symbols

β_i	Mass transport coefficient [1/m]
η_{cat}	Catalyst efficiency [–]
η_{ext}	External catalyst efficiency [–]
η_{int}	Internal catalyst efficiency [–]
θ_i	Surface coverage [–]
ρ_j	Catalyst density [kg/m^3]
Φ_M	Modified Thiele modulus [–]

REFERENCES

[1] Stocker TF, Qin D, Plattner G-K, Tignor MMB, Allen SK, Boschung J, et al. Climate change 2013 the physical science basis: working group I contribution to the fifth assessment report of the intergovernmental Panel on climate change. Cambridge University Press; 2013.

[2] Bundestag WDD. Anthropogener Treibhauseffekt und Klimaänderungen - darstellung des gegenwärtigen wissenschaftlichen Erkenntnisstandes. 2017.

[3] Paris agreement. United Nations Framework Convention on Climate Change (UNFCCC); 2015.

[4] Zahlen und Fakten Energiedaten - nationale und Internationale Entwicklung. Federal Ministry of Economics (BMWi); 2020.

[5] Hermesmann M, Grubel K, Scherotzki L, Müller TE. Promising pathways: the geographic and energetic potential of power-to-x technologies based on regeneratively obtained hydrogen. Renew Sustain Energy Rev 2021;138:110644.

[6] Schemme S, Samsun RC, Peters R, Stolten D. Power-to-fuel as a key to sustainable transport systems - an analysis of diesel fuels produced from CO2 and renewable electricity. Fuel 2017;205:198–221.

[7] Skov IR, Schneider N. Incentive structures for power-to-X and e-fuel pathways for transport in EU and member states. Energy Pol 2022;168:113121.

[8] Zubel To M, Heuser B, Herudek C, Maas H, Willems W. Dme - a sustainable fuel solution for clean and closed CO2-cycle-mobility for CI. Berlin, Heidelberg: Springer Vieweg; 2019.

[9] Park SH, Lee CS. Combustion performance and emission reduction characteristics of automotive DME engine system (vol 39, pg 147, 2013). Prog Energy Combust Sci 2013;39:606.

[10] Thomas G, Feng B, Veeraragavan A, Cleary MJ, Drinnan N. Emissions from DME combustion in diesel engines and their implications on meeting future emission norms: a review. Fuel Process Technol 2014;119:286–304.

[11] Lee SB, Cho W, Park DK, Yoon ES. Simulation of fixed bed reactor for dimethyl ether synthesis. Kor J Chem Eng 2006;23:522–30.

[12] Azizi Z, Rezaeimanesh M, Tohidian T, Rahimpour MR. Dimethyl ether: a review of technologies and production challenges. Chem Eng Process 2014;82:150–72.

[13] Chen W-H, Hsu C-L, Wang X-D. Thermodynamic approach and comparison of two-step and single step DME (dimethyl ether) syntheses with carbon dioxide utilization. Energy 2016;109:326–40.

[14] Manfred Müller UH. Dimethyl ether. Ullmann's Encyclopedia of Industrial Chemistry 2000;11:305–8.

[15] Tomkins P, Müller T. Evaluating the carbon inventory, carbon fluxes and carbon cycles for a long-term sustainable world. Green Chem 2019;21:3994–4013.

[16] Hermesmann M, Müller T. Green, turquoise, blue, or grey? Environmentally friendly hydrogen production in transforming energy systems. Prog Energy Combust Sci 2022;90:100996.

[17] Tsiklios C, Hermesmann M, Müller T. Hydrogen transport in large-scale transmission pipeline networks: thermodynamic and environmental assessment of repurposed and new pipeline configurations. Appl Energy 2022;327:120097.

[18] Renk C. Die einstufige Dimethylether-Synthese aus Synthesegas. Universität Karlsruhe; 2009.

[19] Pontzen F, Liebner W, Gronemann V, Rothaemel M, Ahlers B. CO2-based methanol and DME - efficient technologies for industrial scale production. Catal Today 2011;171:242–50.

[20] Otto A. Chemische, verfahrenstechnische und ökonomische Bewertung von Kohlendioxid als Rohstoff in der chemischen Industrie [E-Book]. Zentralbibliothek: Jülich: Forschungszentrum; 2015.

[21] Moser P, Wiechers G, Schmidt S, Stahl K, Majid M, Bosser S, et al. Demonstrating the CCU-chain and sector coupling as part of ALIGN-CCUS - dimethyl ether from CO2 as chemical energy storage, fuel and feedstock for industries. In: 14th international conference on greenhouse gas control technologies. Melbourne, Australia: GHGT-14; 2018.

[22] Frusteri F, Migliori M, Cannilla C, Frusteri L, Catizzone E, Aloise A, et al. Direct CO2-to-DME hydrogenation reaction: new evidences of a superior behaviour of FER-based hybrid systems to obtain high DME yield. J CO2 Util 2017;18:353–61.

[23] Alvarez A, Bansode A, Urakawa A, Bavykina AV, Wezendonk TA, Makkee M, et al. Challenges in the greener production of formates/formic acid, methanol, and DME by heterogeneously catalyzed CO2 hydrogenation processes. Chem Rev 2017;117:9804–38.

[24] Poto S, Vink T, Oliver P, Gallucci F, Neira d'Angelo MF. Techno-economic assessment of the one-step CO2 conversion to dimethyl ether in a membrane-assisted process. J CO2 Util 2023;69:102419.

[25] Park H, Bae JW, Kim G, Park M-J. Techno-economic analysis of the integrated DME production process: effects of different separation trains and recycling strategies. Kor J Chem Eng 2022;39:2925–34.

[26] Hamedi H, Brinkmann T. Valorization of CO2 to DME using a membrane reactor: a theoretical comparative assessment from the equipment to flowsheet level. Chemical Engineering Journal Advances 2022;10:100249.

[27] Bozzano G, Manenti F. Efficient methanol synthesis: perspectives, technologies and optimization strategies. Prog Energy Combust Sci 2016;56:71–105.

[28] Bercic G, Levec J. Catalytic dehydration of methanol to dimethyl ether - kinetic investigation and reactor simulation. Ind Eng Chem Res 1993;32:2478–84.
[29] Ng KL, Chadwick D, Toseland BA. Kinetics and modelling of dimethyl ether synthesis from synthesis gas. Chem Eng Sci 1999;54:3587–92.
[30] Farsi M, Jahanmiri A, Eslamloueyan R. Modeling and optimization of MeOH to DME in isothermal fixed-bed reactor. Int J Chem React Eng 2010;8.
[31] Song D, Cho W, Lee G, Park DK, Yoon ES. Numerical analysis of a pilot-scale fixed-bed reactor for dimethyl ether (DME) synthesis. Ind Eng Chem Res 2008;47:4553–9.
[32] Erena J, Sierra I, Aguayo AT, Ateka A, Olazar M, Bilbao J. Kinetic modelling of dimethyl ether synthesis from (H-2 + CO2) by considering catalyst deactivation. Chem Eng J 2011;174:660–7.
[33] Hadipour A, Sohrabi M. Synthesis of some bifunctional catalysts and determination of kinetic parameters for direct conversion of syngas to dimethyl ether. Chem Eng J 2008;137:294–301.
[34] Hadipour A, Sohrabi M. Kinetic parameters and dynamic modeling of a reactor for direct conversion of synthesis gas to dimethyl ether. J Ind Eng Chem 2007;13:558–65.
[35] Ateka A, Perez-Uriarte P, Gamero M, Erena J, Aguayo AT, Bilbao J. A comparative thermodynamic study on the CO2 conversion in the synthesis of methanol and of DME. Energy 2017;120:796–804.
[36] Vakili R, Eslamloueyan R. Design and optimization of a fixed bed reactor for direct dimethyl ether production from syngas using differential evolution algorithm. Int J Chem React Eng 2013;11.
[37] Vakili R, Eslamloueyan R. Optimal design of an industrial scale dual-type reactor for direct dimethyl ether (DME) production from syngas. Chem Eng Process 2012;62:78–88.
[38] De Falco M, Capocelli M, Centi G. Dimethyl ether production from CO2 rich feedstocks in a one-step process: thermodynamic evaluation and reactor simulation. Chem Eng J 2016;294:400–9.
[39] Otalvaro ND, Sogne G, Delgado KH, Wild S, Pitter S, Sauer J. Kinetics of the direct DME synthesis from CO 2 rich syngas under variation of the CZA-to-γ-Al 2 O 3 ratio of a mixed catalyst bed. RSC Adv 2021;11:24556–69.
[40] McBride K, Turek T, Güttel R. Direct dimethyl ether synthesis by spatial patterned catalyst arrangement: a modeling and simulation study. AIChE J 2012;58:3468–73.
[41] Moradi F, Kazemeini M, Fattahi M. A three dimensional CFD simulation and optimization of direct DME synthesis in a fixed bed reactor. Petrol Sci 2014;11:323–30.
[42] Iliuta I, Larachi F, Fongarland P. Dimethyl ether synthesis with in situ H2O removal in fixed-bed membrane reactor: model and simulations. Ind Eng Chem Res 2010;49:6870–7.
[43] Poto S, Gallucci F, Fernanda Neira d'Angelo M. Direct conversion of CO2 to dimethyl ether in a fixed bed membrane reactor: influence of membrane properties and process conditions. Fuel 2021;302:121080.
[44] De Falco M, Capocelli M, Basile A. Selective membrane application for the industrial one-step DME production process fed by CO2 rich streams: modeling and simulation. Int J Hydrogen Energy 2017;42:6771–86.
[45] Koybasi HH, Avci AK. Numerical analysis of CO2-to-DME conversion in a membrane microchannel reactor. Ind Eng Chem Res 2022;61:10846–59.
[46] Guffanti S, Visconti CG, van Kampen J, Boon J, Groppi G. Reactor modelling and design for sorption enhanced dimethyl ether synthesis. Chem Eng J 2021;404:126573.
[47] Iranshahi D, Saeedi R, Azizi K. Maximization of dimethyl ether production from synthesis gas by obtaining optimum temperature profile and water removal. Fuel 2017;190:386–95.
[48] Samimi F, Rahimpour MR, Shariati A. Development of an efficient methanol production process for direct CO2 hydrogenation over a Cu/ZnO/Al2O3 catalyst. Catalysts 2017;7.
[49] Graaf G, Sijtsema P, Stamhuis E, Joosten G. Chemical equilibria in methanol synthesis. Chem Eng Sci 1986;41:2883–90.
[50] Diep BT, Wainwright MS. Thermodynamic equilibrium constants for the methanol-dimethyl ether-water system. J Chem Eng Data 1987;32:330–3.
[51] Graaf GH. The syntheis of methanol in gas-solid and gas-slurry reactors, vol. 1988. PhD Thesis; 2016.
[52] Portha JF, Parkhomenko K, Kobl K, Roger AC, Arab S, Commenge JM, et al. Kinetics of methanol synthesis from carbon dioxide hydrogenation over copper-zinc oxide catalysts. Ind Eng Chem Res 2017;56:13134–46.
[53] Wilkinson SK, van de Water LGA, Miller B, Simmons MJH, Stitt EH, Watson MJ. Understanding the generation of methanol synthesis and water gas shift activity over copper-based catalysts – a spatially resolved experimental kinetic study using steady and non-steady state operation under CO/CO2/H2 feeds. J Catal 2016;337:208–20.
[54] Meyer JJ, Tan P, Apfelbacher A, Daschner R, Hornung A. Modeling of a methanol synthesis reactor for storage of renewable energy and conversion of CO2 - comparison of two kinetic models. Chem Eng Technol 2016;39:233–45.
[55] Peter M, Fichtl MB, Ruland H, Kaluza S, Muhler M, Hinrichsen O. Detailed kinetic modeling of methanol synthesis over a ternary copper catalyst. Chem Eng J 2012;203:480–91.
[56] Askari F, Rahimpour MR, Jahanmiri A, Mostafazadeh AK. Dynamic simulation and optimization of a dual-type methanol reactor using genetic algorithms. Chem Eng Technol 2008;31:513–24.
[57] Rezaei N, Jahanmiri A, Moghtaderi B, Rahimpour MR. A comparison of homogeneous and heterogeneous dynamic models for industrial methanol reactors in the presence of catalyst deactivation 2005.
[58] VandenBussche KM, Froment GF. A steady-state kinetic model for methanol synthesis and the water gas shift reaction on a commercial Cu/ZnO/Al2O3 catalyst. J Catal 1996;161:1–10.
[59] Suzana Y, Anh NP, Zabiri H. A simulation study of an industrial methanol reactor based on simplified steady-state model 2010.
[60] Seidel C, Jorke A, Vollbrecht B, Seidel-Morgenstern A, Kienle A. Kinetic modeling of methanol synthesis from renewable resources. Chem Eng Sci 2018;175:130–8.
[61] Ergun S. Fluid flow through packed columns. Chem Eng Prog 1952;48:89–94.
[62] ANSYS FLUENT theory guide V17. vol. 2. 2016.
[63] Henkel TA. Modellierung von Reaktion und Stofftransport in geformten Katalysatoren am Beispiel der Methanolsynthese. Dissertation München: TU München; 2011.
[64] Lommerts BJ, Graaf GH, Beenackers AACM. Mathematical modeling of internal mass transport limitations in methanol synthesis. Chem Eng Sci 2000;55:5589–98.

[65] Thiele EW. Relation between catalytic activity and size of particle. Ind Eng Chem 1939;31:916–20.
[66] Wessling M. Begleitende Unterlagen zur Veranstaltung Chemische Verfahrenstechnik. 2017.
[67] Cussler EL. Fundamentals of mass transfer. In: Cussler EL, editor. Diffusion: mass transfer in fluid systems. 3 ed. Cambridge: Cambridge University Press; 2009. p. 237–73.
[68] Dieterich V, Buttler A, Hanel A, Spliethoff H, Fendt S. Power-to-liquid via synthesis of methanol, DME or Fischer–Tropsch-fuels: a review. Energy Environ Sci 2020;13:3207–52.
[69] Behr A, Agar D, Jörissen J. Einführung in die Technische Chemie 2010.
[70] Manenti F, Leon-Garzon AR, Ravaghi-Ardebili Z, Pirola C. Systematic staging design applied to the fixed-bed reactor series for methanol and one-step methanol/dimethyl ether synthesis. Appl Therm Eng 2014;70:1228–37.
[71] Soave G. Equilibrium constants from a modified redlich-kwong equation of state. Chem Eng Sci 1972;27:1197.
[72] Redlich O, Kwong JNS. On the thermodynamics of solutions. V. An equation of state. Fugacities of gaseous solutions. Chem Rev 1949;44:233–44.
[73] Bercic G, Levec J. Catalytic dehydration of methanol to dimethyl ether. Kinetic investigation and reactor simulation. Ind Eng Chem Res 1993;32:2478–84.
[74] Ghavipour M, Behbahani RM. Fixed-bed reactor modeling for methanol to dimethyl ether (DME) reaction over gamma-Alumina using a new practical reaction rate model. J Ind Eng Chem 2014;20:1942–51.
[75] Kurzina IA, Reshetnikov SI, Karakchieva NI, Kurina LN. Direct synthesis of dimethyl ether from synthesis gas: experimental study and mathematical modeling. Chem Eng J 2017;329:135–41.
[76] Rohde MP, Schaub G, Khajavi S, Jansen JC, Kapteijn F. Fischer–Tropsch synthesis with in situ H2O removal – directions of membrane development. Microporous Mesoporous Mater 2008;115:123–36.
[77] Gorbe J, Lasobras J, Francés E, Herguido J, Menéndez M, Kumakiri I, et al. Preliminary study on the feasibility of using a zeolite A membrane in a membrane reactor for methanol production. Separation and Purification Technology 2018;200:164–8.